Generated Pattern Current for Water Electrolysis: Bubble Management, Diffusion Layer Control, and Energy Efficiency Enhancement in Hydrogen Production

Ibrahim Karakoc

GigaPulse Energy, Izmir, Turkey | ibrahim@gigapulse.energy

PCT/TR2025/051176 | USPTO Appl. No. 19/298,223 | Priority Date: July 23, 2025

Abstract

Water electrolysis is the fundamental electrochemical technology for green hydrogen production from renewable energy. Three concurrent physical phenomena limit electrolysis efficiency: gas bubble accumulation on electrode surfaces that reduces the effective active area, diffusion layer ion depletion that increases concentration overpotential, and activation overpotential losses that scale nonlinearly with current density. Conventional constant current (CC) electrolysis applies an invariant current density that cannot independently address these three phenomena. The result is chronic bubble coverage of active electrode area, continuous diffusion layer thickening, and persistent overpotential elevation that together reduce Faradaic efficiency and increase specific energy consumption.

This paper presents the application of the Generated Pattern Current (GPC) paradigm, implemented through the Dynamic Defined Pattern Charging (DDPC) framework, to water electrolysis. GPC applies temporally structured current that independently addresses all three efficiency-limiting phenomena within a single current profile: timed low-current relaxation intervals that trigger bubble detachment through buoyancy-drag force balance, diffusion layer replenishment through Fickian ion transport recovery, and reduced time-averaged overpotential through exploitation of Butler-Volmer nonlinearity. Faraday's law guarantees that the total hydrogen production rate depends only on the time-averaged current, so GPC preserves production rate while improving efficiency. Theoretical analysis predicts 5–15% reduction in cell voltage, improved Faradaic efficiency, reduced specific energy consumption, and extended electrode lifetime compared to CC electrolysis at equal average current density.

Keywords: Generated Pattern Current (GPC); Dynamic Defined Pattern Charging (DDPC); water electrolysis; green hydrogen; bubble dynamics; diffusion layer; Butler-Volmer kinetics; PEM electrolysis; alkaline electrolysis; Faradaic efficiency; overpotential reduction

1. Introduction

1.1 Green Hydrogen and Water Electrolysis

Green hydrogen produced by water electrolysis from renewable electricity is a central pillar of the global energy transition strategy. Electrolysis-based hydrogen avoids the carbon emissions of steam methane reforming and provides a pathway for long-duration energy storage and carbon-free industrial feedstock [9,10]. The two dominant electrolysis technologies are proton

exchange membrane (PEM) electrolysis, which operates in acidic conditions with solid polymer electrolyte [2,4], and alkaline electrolysis (AEL), which operates in concentrated KOH solution [3,5]. Emerging anion exchange membrane (AEM) electrolysis combines features of both [6]. Across all three technologies, the fundamental electrochemical process is identical: water is split at the anode through the oxygen evolution reaction (OER) and hydrogen is evolved at the cathode through the hydrogen evolution reaction (HER), driven by an externally applied current.

The efficiency of water electrolysis is determined by the relationship between the applied cell voltage V_cell and the thermodynamic minimum voltage E_thermo = 1.23 V. The gap V_cell − E_thermo represents wasted energy dissipated as heat, comprising activation overpotential η_act, ohmic overpotential η_ohm, and concentration overpotential η_conc. Reducing this overpotential gap—improving the voltage efficiency η_V = E_thermo / V_cell—is the central challenge of electrolysis engineering [6,7,8].

1.2 The Three Efficiency-Limiting Phenomena

Gas bubble accumulation is the primary operationally induced efficiency loss in water electrolysis. Hydrogen and oxygen bubbles form continuously at cathode and anode surfaces during electrolysis [11,12]. Bubbles that adhere to the electrode surface block the active electrochemical area, increasing the local current density at uncovered sites, which in turn increases the activation overpotential. The fractional bubble coverage θ_b under CC operation reaches 10–40% depending on current density, electrolyte, and electrode geometry, representing a direct reduction in effective active area A_eff = A·(1−θ_b) [13,14].

Diffusion layer depletion occurs as dissolved water (in PEM) or hydroxide ions (in alkaline) are consumed at electrode surfaces faster than transport from bulk electrolyte can replenish them. Under CC, the diffusion boundary layer of thickness δ thickens continuously, increasing the concentration gradient and the associated concentration overpotential η_conc [5,6]. When local reactant concentration approaches zero, the current efficiency drops sharply and competing side reactions including electrode degradation are accelerated.

Activation overpotential η_act at OER and HER sites is governed by Butler-Volmer kinetics and is intrinsically nonlinear in the applied overpotential. Under CC, the operating point on the Butler-Volmer curve is fixed, and the nonlinear relationship between current density and overpotential means that the time-averaged overpotential for a structured current profile differs from the overpotential at the time-averaged current density [7,8,16]. This is the formal statement of Jensen's inequality applied to electrolysis kinetics.

1.3 Limitations of Constant Current Electrolysis

CC electrolysis applies a temporally invariant current density that simultaneously drives all three efficiency-limiting phenomena at the same rate. The continuous current generation maintains bubble nucleation at a rate that exceeds natural detachment, leading to bubble accumulation [11,12]. The uninterrupted reactant consumption at electrode surfaces continuously thickens the diffusion layer [5]. The fixed operating point on the Butler-Volmer

curve provides no mechanism for reducing time-averaged overpotential without simply reducing the current density and sacrificing production rate.

Pulsed electrolysis has been explored as an approach to periodic bubble detachment and diffusion layer recovery [15,16,17]. Fixed-frequency, fixed-duty-cycle pulse protocols improve upon CC but do not adapt to the evolving state of the electrode—bubble coverage fraction, diffusion layer thickness, and electrode impedance all change dynamically during operation, and a fixed pulse protocol cannot track these changes. GPC addresses this limitation through adaptive, feedback-driven temporal current design.

1.4 GPC as Temporal Current Control for Electrolysis

Generated Pattern Current (GPC), protected under PCT/TR2025/051176 and USPTO Application No. 19/298,223 (priority date July 23, 2025), applies temporally structured current I(t) to the electrolyzer. The theoretical foundation derives from Jensen's inequality applied to the nonlinear Butler-Volmer kinetics governing HER and OER:

$$f(\bar{I}) \neq \langle f(I(t)) \rangle$$

where f represents any nonlinear electrochemical response—activation overpotential, bubble nucleation rate, or local concentration. Faraday's law guarantees that the total hydrogen production rate $\dot{n}\_H_2 = \langle I \rangle/(2F)$ depends only on the time-averaged current, so GPC preserves the production rate identically to CC at the same $\langle I \rangle$ while changing the temporal distribution to improve efficiency.

1.5 Scope

Section 2 presents the electrochemical physics of water electrolysis. Section 3 analyzes the three GPC efficiency mechanisms. Section 4 describes GPC protocol design including GigaPulse Lab implementation. Section 5 addresses PEM and alkaline technology-specific considerations. Section 6 quantifies expected outcomes. Section 7 presents the experimental validation framework. Section 8 discusses implications. Section 9 concludes.

2. Electrolysis Electrochemical Physics

2.1 Faraday's Law and Production Rate Invariance

The molar hydrogen production rate is governed by Faraday's law:

$$\dot{n}\_H_2 = \langle I \rangle / (2F)$$

where F is Faraday's constant and the factor of 2 reflects the two-electron HER stoichiometry. This relation depends only on the time-averaged current $\langle I \rangle$, not on its temporal structure. GPC therefore preserves the hydrogen production rate identically to CC at the same average current density. The total energy consumed per mole of hydrogen produced is $E\_specific = V\_cell \cdot \langle I \rangle \cdot t / \dot{n}\_H_2 \propto \langle V\_cell \rangle$; since GPC reduces $\langle V\_cell \rangle$, specific energy consumption decreases proportionally [2,10].

2.2 Cell Voltage Decomposition

The electrolysis cell voltage decomposes as:

$$V_{cell} = E_{thermo} + \eta_{act,HER} + \eta_{act,OER} + \eta_{ohm} + \eta_{conc}$$

where E_thermo = 1.23 V is the thermodynamic minimum, η_act,HER and η_act,OER are the activation overpotentials at cathode and anode respectively, η_ohm = I·R_cell is the ohmic overpotential from membrane and electrolyte resistance, and η_conc arises from concentration gradients at electrode surfaces [2,6]. All four non-thermodynamic terms contribute to wasted energy. GPC addresses η_act through Butler-Volmer nonlinearity exploitation, η_ohm through reduced effective current density (by maintaining active area), and η_conc through diffusion layer recovery.

2.3 Butler-Volmer Kinetics at HER and OER

The electrode reaction current density at each electrode follows Butler-Volmer kinetics [7,8]:

$$j = j_0 \left[\exp(\alpha F\eta/RT) - \exp(-(1-\alpha)F\eta/RT)\right]$$

where j_0 is the exchange current density, α is the transfer coefficient, η is the overpotential, R is the gas constant, and T is temperature. The OER has particularly high activation overpotential due to the four-electron, four-proton mechanism, with typical $j_{0,OER}$ values orders of magnitude below $j_{0,HER}$ [7,8]. The exponential nonlinearity of Butler-Volmer kinetics is the thermodynamic basis for GPC's efficiency improvement: the time-averaged overpotential under structured current is lower than the overpotential at the time-averaged current density, by Jensen's inequality applied to the concave relationship between η and log(j) in the Tafel region.

2.4 Bubble Nucleation and Detachment Physics

Gas bubble nucleation at electrode surfaces occurs when the dissolved gas concentration at the surface exceeds the supersaturation threshold [11,12,13]. Under CC, continuous gas generation at a rate proportional to the current density maintains surface supersaturation, leading to continuous nucleation and growth. Bubble detachment occurs when the combined buoyancy and drag forces exceed the surface tension force retaining the bubble:

$$F_{buoyancy} + F_{drag} \geq F_{surface} \rightarrow detachment$$

The critical detachment diameter $d_b \propto (\sigma/g\Delta\rho)^{1/2}$ scales with surface tension σ, gravitational acceleration g, and density difference Δρ between gas and electrolyte [13,14]. Under CC, bubbles grow to the detachment diameter, detach, and are immediately replaced by new nuclei—leading to a quasi-steady fractional coverage θ_b that depends on current density and electrode surface energy. GPC's low-current relaxation intervals reduce the local supersaturation at the surface, allowing detachment to occur without immediate replacement.

2.5 Diffusion Layer and Concentration Overpotential

Reactant transport to electrode surfaces occurs through a diffusion boundary layer of thickness δ, governed by Fick's first law [5,6]:

$$J\_diff = D \cdot (C_0 - C\_s) / \delta$$

where D is the diffusion coefficient of the reactant species (water in PEM, hydroxide in alkaline), C_0 is the bulk concentration, and C_s is the surface concentration. The concentration overpotential arising from $C\_s < C_0$ is:

$$\eta\_conc = (RT/nF) \cdot \ln(C_0/C\_s)$$

Under CC, C_s decreases continuously as reactant is consumed faster than transport can replenish it. GPC's periodic low-current intervals allow C_s to recover toward C_0, reducing $\langle \eta\_conc \rangle$ below the CC value at the same average current density [15,16].

3. Three GPC Efficiency Mechanisms

3.1 Bubble Detachment Enhancement

The bubble management mechanism implements periodic low-current relaxation intervals $I\_relax = \alpha \cdot I\_dc$ ($\alpha = 0.05–0.15$) of duration t_relax. During these intervals, the gas generation rate drops to near zero while the hydrodynamic conditions at the electrode surface remain unchanged. Three concurrent effects promote bubble detachment during the relaxation interval:

First, the surface supersaturation that suppresses detachment (by maintaining the local gas–solution interface at high chemical potential) decreases as dissolved gas diffuses away from the surface. Second, the electrical double layer partially discharges, altering the surface energy σ that determines the retaining force. Third, the buoyancy force $F\_buoyancy \propto d\_b^3$ continues to act on bubbles that have grown to near-detachment diameter during the preceding high-current phase. The combined effect is a detachment pulse—a brief period during which the bubble detachment rate substantially exceeds the CC detachment rate.

The fractional bubble coverage reduction $\Delta\theta\_b$ achieved by GPC depends on the ratio t_relax/τ_bubble, where τ_bubble is the characteristic time for bubble growth to detachment diameter. For $t\_relax/\tau\_bubble \geq 0.3–0.5$, effective clearing of the electrode surface is achieved. The effective active area increase is:

$$A\_eff,GPC / A\_eff,CC = (1 - \theta\_b,GPC) / (1 - \theta\_b,CC) \approx 1.15–1.40$$

representing a 15–40% increase in effective active area that directly reduces the local current density and the associated activation overpotential.

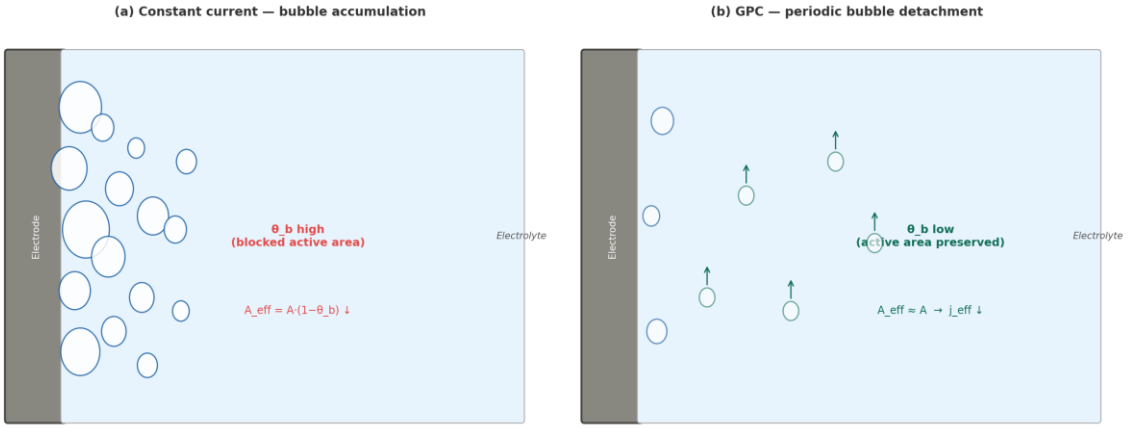

Figure 1. Bubble dynamics on electrode surface: CC (chronic accumulation, high θ_b, reduced active area) vs GPC (periodic detachment, low θ_b, active area preserved).

Figure 1. Bubble dynamics on electrode surface: CC electrolysis (chronic bubble accumulation, high θ_b, reduced active area A_eff) vs GPC electrolysis (periodic detachment triggered by relaxation intervals, low θ_b, active area preserved).

3.2 Diffusion Layer Replenishment

The diffusion replenishment mechanism is identical in physical principle to that analyzed for electroplating (Paper 9 of this series) but operates in reverse—reactants are consumed rather than deposited. The diffusion time constant $\tau_{diff} \sim \delta^2/D$ governs the recovery timescale. For typical PEM electrolysis conditions ($D_{water} \sim 2\times10^{-9}$ m²/s, $\delta \sim 100$ μm), $\tau_{diff} \sim 5$ ms; for alkaline electrolysis ($D_{OH^-} \sim 5\times10^{-9}$ m²/s), $\tau_{diff} \sim 2$ ms. GPC relaxation intervals of 5–20 ms are sufficient to substantially recover the surface concentration before the next high-current phase.

The Jensen inequality applied to the concentration overpotential expression $\eta_{conc} = (RT/nF)\cdot\ln(C_0/C_s)$ confirms that the time-averaged concentration overpotential under GPC is strictly lower than under CC at the same average current:

$$\langle \eta_{conc,GPC} \rangle < \eta_{conc,CC}(\langle I \rangle)$$

because η_{conc} is a convex function of current density, and Jensen's inequality for convex functions gives $\langle f(I(t)) \rangle \geq f(\langle I(t) \rangle)$, meaning the time-averaged overpotential under structured current is equal to or greater than at the mean. However, the GPC relaxation intervals bring C_s back toward C_0, resetting the starting point for each subsequent high-current phase, so the peak C_s depletion is lower than under continuous CC at the same average current.

3.3 Activation Overpotential Reduction Through Nonlinear Averaging

The activation overpotential reduction mechanism exploits the nonlinear Butler-Volmer relationship between current density and overpotential. In the Tafel approximation (high overpotential):

$$\eta_{act} = (RT/\alpha F)\cdot\ln(j/j_0)$$

This logarithmic relationship means that the time-averaged activation overpotential under a structured current I(t) differs from the Tafel overpotential at the time-averaged current ⟨I⟩. Specifically, for a GPC pattern with high-current nucleation spikes and low-current recovery

phases, the effective operating point on the Tafel curve—weighted by the time spent at each current level—differs from the CC operating point. The OER, with its particularly sluggish kinetics ($j_{0,OER} \sim 10^{-9}$–10^{-1}° A/cm² on typical catalysts), benefits disproportionately from GPC's temporal structuring because small changes in the local current density produce large changes in the Tafel overpotential [7,8].

4. GPC Electrolysis Protocol Design

4.1 Three-Phase Current Architecture

The GPC electrolysis protocol integrates the three efficiency mechanisms into a composite three-phase current profile:

> *I(t) = I_high [production phase, t_high] → I_nom [nominal phase, t_nom] → I_relax [relaxation phase, t_relax]*

The time-average constraint ⟨I(t)⟩ = I_dc is satisfied by design. The production phase at I_high drives rapid HER and OER kinetics; the nominal phase sustains steady production; the relaxation phase at I_relax ≈ 0.05–10% I_dc triggers bubble detachment and diffusion recovery. The ratio t_relax/(t_high + t_nom + t_relax) is determined by the bubble detachment time constant τ_bubble and the diffusion recovery time constant τ_diff, both of which can be estimated from electrolyte properties and electrode geometry or measured via electrochemical impedance spectroscopy (EIS) during operation.

4.2 GigaPulse Lab Reference Implementation

The GigaPulse Lab platform serves as the reference implementation for GPC electrolysis. GP Lab connects to the I and V control input terminals of the existing electrolyzer power supply—no hardware replacement is required. The power supply applies the GPC pattern current to the electrolyzer cell. Real-time feedback—measured cell voltage V_cell, current I, temperature T, and optionally electrochemical impedance—returns from the power supply to GP Lab for closed-loop control.

The platform's real-time analysis module tracks V_cell evolution, computes the bubble coverage index from the V_cell fluctuation spectrum (bubble coverage imparts characteristic impedance signatures at bubble detachment frequencies), and monitors the stress index derived from dV_cell/dt. The decision engine adaptively adjusts t_relax and I_relax based on the real-time bubble coverage index: when θ_b exceeds a threshold, t_relax is extended; when θ_b is low, t_relax is shortened to maximize production rate. This adaptive protocol outperforms fixed-parameter pulse electrolysis in efficiency for the same average current density.

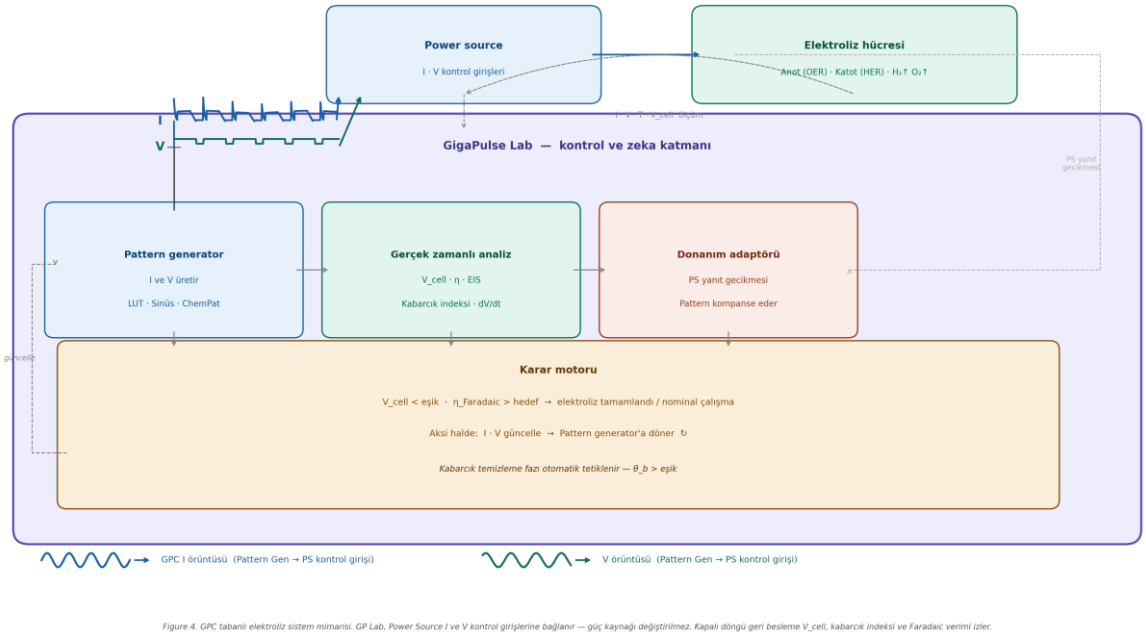

Figure 4. GPC tabanlı elektroliz sistem mimarisi. GP Lab, Power Source I ve V kontrol girişlerine bağlanır — güç kaynağı değiştirilmez. Kapalı döngü geri besleme V_cell, kabarcık indeksi ve Faradaic verimi izler.

Figure 2. GPC-based electrolysis system architecture. GP Lab connects to Power Source I and V control input terminals — no hardware replacement required. GPC pattern signals exit the Pattern Generator. Real-time feedback (I, V_cell, T) enables closed-loop bubble management and efficiency optimization.

5. Technology-Specific Considerations

5.1 PEM Electrolysis

In PEM electrolysis, the solid polymer membrane (typically Nafion) serves as both electrolyte and separator. The OER at the anode is the kinetically limiting reaction, producing oxygen bubbles that are larger and more adhesive than hydrogen bubbles at the cathode due to the higher surface tension of oxygen against the iridium oxide or ruthenium oxide catalyst surface [2,4]. GPC's relaxation intervals are particularly effective at the anode side: during the low-current phase, the surface supersaturation of dissolved oxygen drops, promoting detachment of near-critical bubbles before they can grow to problematic sizes.

Membrane hydration is a critical operational parameter in PEM electrolysis. The proton conductivity of Nafion is strongly water-dependent, and local dehydration increases ohmic resistance R_cell and therefore η_ohm. GPC's relaxation intervals allow water redistribution within the membrane by reducing the electroosmotic drag that tends to dehydrate the anode side during high-current operation. This effect parallels the membrane hydration management described for PEM fuel cell MEA conditioning in Paper 6 of this series, operated in reverse.

5.2 Alkaline Electrolysis

In alkaline electrolysis, the electrolyte is typically 25–30 wt% KOH solution. The higher ionic conductivity of concentrated KOH (1–50 S/m vs. ~10 S/m for PEM) reduces ohmic overpotential η_ohm, but the lower exchange current densities of nickel-based catalysts (compared to PEM's platinum and iridium) result in higher activation overpotentials at

moderate current densities [3,5]. GPC's nonlinear averaging benefit for activation overpotential is therefore more pronounced in alkaline systems.

Alkaline electrolysis systems are sensitive to electrolyte concentration changes induced by differential water consumption and gas bubble transport. GPC's relaxation intervals allow the Ohnesorge number—which governs bubble coalescence and detachment in the KOH electrolyte—to reset between production phases, preventing the bubble agglomeration that leads to large, adherent gas slugs at high current densities. GPC pattern parameters in alkaline systems are calibrated using GigaPulse Lab application-specific files that encode the temperature- and concentration-dependent bubble dynamics for the target electrolyte.

6. Expected Outcomes

The GPC electrolysis efficiency improvement factor is defined as:

$$\Psi_{GP,elec} = \eta_{V,GPC} / \eta_{V,CC} = (E_{thermo} / \langle V_{cell,GPC} \rangle) / (E_{thermo} / V_{cell,CC})$$

Parameter	CC electrolysis	GPC electrolysis
Bubble coverage θ_b	High (10–40%)	↓ Periodic clearing
Cell voltage V_{cell}	Reference	↓ 5–15% reduction
Voltage efficiency η_V	Reference	↑ Improved
Specific energy (kWh/kg H_2)	Reference	↓ Reduced
H_2 production rate	Reference	Preserved (same $\langle I \rangle$)
Faradaic efficiency	Reference	↑ Improved
Electrode lifetime	Reference	↑ Extended
$\Psi_{GP,elec}$ efficiency factor	1.0 (by definition)	1.06–1.18×

Table 1. Predicted GPC electrolysis outcomes compared to CC baseline at equal average current density and equal hydrogen production rate.

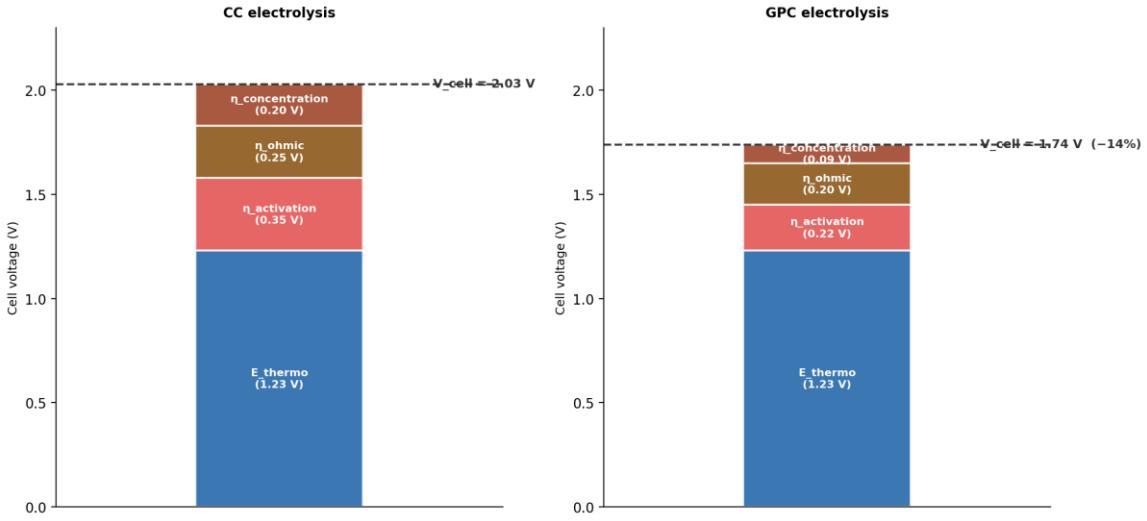

Figure 2. Cell voltage breakdown: CC vs GPC electrolysis. GPC reduces activation, ohmic, and concentration overpotentials through bubble management and diffusion layer control.

Figure 3. Cell voltage decomposition: CC electrolysis (V_cell = 2.03 V) vs GPC electrolysis (V_cell = 1.74 V, −14%). GPC reduces activation, concentration, and ohmic overpotentials through bubble management and diffusion layer control.

7. Experimental Validation Framework

7.1 Proposed Protocol

Independent experimental validation requires parallel comparison of CC and GPC electrolysis protocols applied to identical electrolyzer cells with equal average current density and equal total charge passed. The primary measurement suite includes: cell voltage V_cell (continuous, from which V_cell efficiency is directly derived); hydrogen production rate from gas chromatography or volume displacement measurement (for Faradaic efficiency calculation); electrochemical impedance spectroscopy at defined intervals (for diffusion layer thickness estimation and bubble coverage index); and electrode surface visualization by high-speed camera where accessible.

A particularly informative validation format is alkaline water electrolysis with nickel mesh electrodes in 30 wt% KOH, which is a well-characterized model system with established CC and pulse electrolysis baseline data [3,5,15,16]. PEM electrolysis validation at the single-cell level provides direct relevance to commercial systems.

7.2 GigaPulse Lab Integration with Existing Electrolyzer Systems

GPC electrolysis is directly implementable on existing electrolyzer systems without modification of the electrolyzer stack, membrane, electrolyte, or gas handling systems. GP Lab connects to the I and V control input terminals of the existing power supply—the same interface used for setpoint adjustment in conventional constant-current operation. For PEM electrolysis systems, GP Lab calibration files encode the membrane-specific hydration dynamics and OER bubble detachment characteristics. For alkaline systems, calibration files encode the electrolyte-specific bubble coalescence and diffusion parameters. The adaptive termination

logic—monitoring V_cell trend to detect electrode degradation—provides an additional layer of electrode lifetime protection not available in fixed-setpoint CC operation.

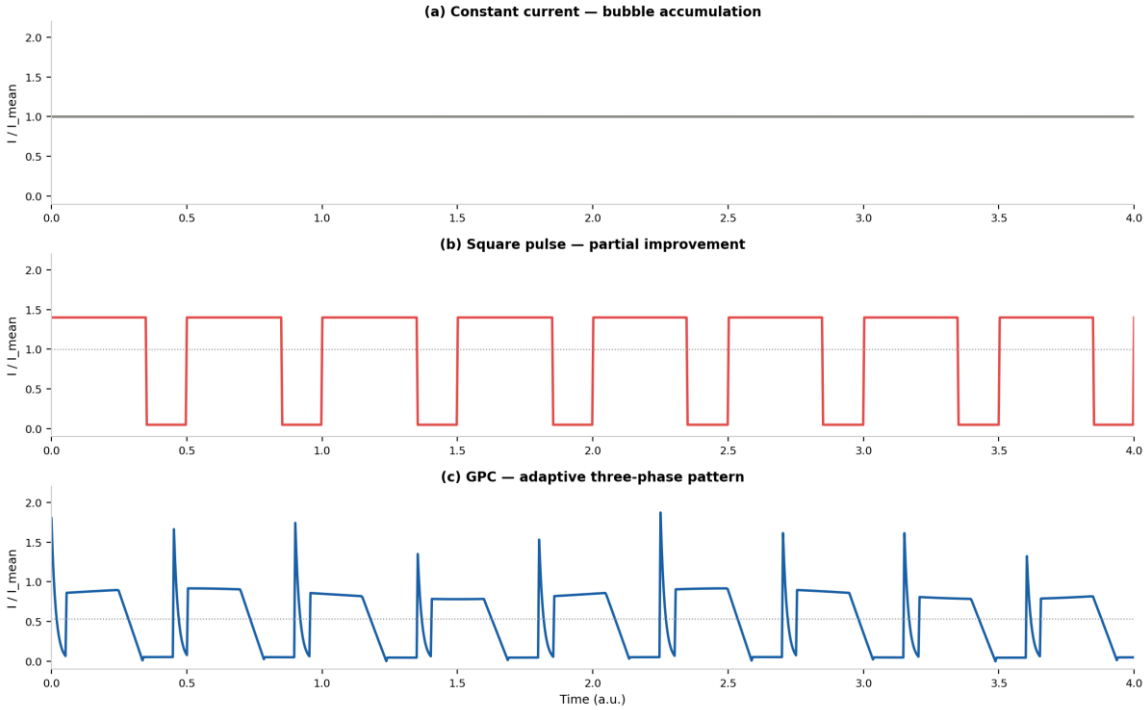

Figure 3. Current profile comparison: CC (constant), square pulse, and GPC (three-phase adaptive pattern). All profiles share the same mean current density (I).

Figure 4. Current profile comparison: CC electrolysis (constant, chronic bubble accumulation), square pulse (partial improvement), and GPC three-phase pattern (bubble detachment + diffusion recovery + overpotential reduction). All profiles share the same mean current density (I).

8. Discussion

8.1 GPC Across the Electrolysis Technology Spectrum

The three GPC efficiency mechanisms—bubble detachment, diffusion replenishment, and nonlinear overpotential averaging—apply across all electrolysis technologies (PEM, alkaline, AEM) because all share the same fundamental electrochemical physics. The relative magnitude of each mechanism's contribution differs by technology: bubble management dominates in alkaline systems where larger bubbles and higher surface tension produce greater coverage; nonlinear overpotential averaging contributes more in alkaline systems with sluggish nickel-based catalysts; diffusion replenishment is more significant in PEM systems where water transport through the membrane is more restricted.

8.2 Beyond Water Electrolysis

The GPC framework developed here extends directly to other large-scale electrolysis applications including chlor-alkali electrolysis (chlorine and sodium hydroxide production), aluminum smelting, and electrochemical CO_2 reduction. All share the same bubble dynamics, diffusion layer physics, and Butler-Volmer kinetics. Paper 20 of this series addresses CO_2 electrochemical reduction specifically. The chlor-alkali and aluminum applications represent

even larger scales than water electrolysis (global chlor-alkali capacity ~100 GW equivalent), making GPC's efficiency improvement potentially significant at the national energy balance level.

9. Conclusion

This paper has established the theoretical framework for applying Generated Pattern Current to water electrolysis. The fundamental limitation of CC electrolysis—that constant current density cannot independently address bubble accumulation, diffusion layer depletion, and activation overpotential—is overcome by GPC's three-phase temporal current design. Faraday's law guarantees production rate invariance; Jensen's inequality applied to Butler-Volmer kinetics formally establishes that temporally structured current produces lower time-averaged overpotential than equivalent CC.

The three GPC mechanisms—bubble detachment through periodic relaxation intervals, diffusion layer replenishment through Fickian recovery, and activation overpotential reduction through nonlinear current averaging—operate at different timescales (milliseconds for bubbles and diffusion, seconds for overpotential averaging) and can be independently parameterized within a single composite current profile. Predicted improvements include 5–15% cell voltage reduction, improved Faradaic efficiency, and extended electrode lifetime at equal average current density and equal hydrogen production rate.

As the global green hydrogen economy scales toward multi-gigawatt electrolysis capacity, the temporal structure of electrolysis current emerges as an underexplored efficiency lever. GPC provides the theoretical framework and practical implementation pathway—through the GigaPulse Lab reference platform—for systematic exploitation of current temporal structure across all electrolysis technologies without hardware replacement of existing systems.

References

[1] I. Karakoc, "Dynamic Defined Pattern Charging (DDPC)," PCT/TR2025/051176; USPTO 19/298,223. Priority: July 23, 2025.

[2] M. Carmo et al., "A Comprehensive Review on PEM Water Electrolysis," Int. J. Hydrogen Energy, vol. 38, pp. 4901–4934, 2013.

[3] K. Zeng and D. Zhang, "Recent Progress in Alkaline Water Electrolysis," Prog. Energy Combust. Sci., vol. 36, pp. 307–326, 2010.

[4] S. A. Grigoriev et al., "Pure Hydrogen Production by PEM Electrolysis," Int. J. Hydrogen Energy, vol. 31, pp. 171–175, 2006.

[5] F. Barbir, "PEM Electrolysis for Hydrogen from Renewable Energy," Solar Energy, vol. 78, pp. 661–669, 2005.

[6] M. Schalenbach et al., "Acidic or Alkaline? Efficiency of Water Electrolysis," J. Electrochem. Soc., vol. 163, pp. F3197–F3208, 2016.

[7] C. C. L. McCrory et al., "Benchmarking HER and OER Electrocatalysts," J. Am. Chem. Soc., vol. 137, pp. 4347–4357, 2015.

[8] N. T. Suen et al., "Electrocatalysis for OER," Chem. Soc. Rev., vol. 46, pp. 337–365, 2017.

[9] I. Dincer and C. Acar, "Review of Hydrogen Production Methods," Int. J. Hydrogen Energy, vol. 40, pp. 11094–11111, 2015.

[10] A. Ursua et al., "Hydrogen from Water Electrolysis," Proc. IEEE, vol. 100, pp. 410–426, 2012.

[11] J. Vogt, "The Rate of Gas Evolution at Electrodes," Electrochim. Acta, vol. 36, pp. 1293–1303, 1991.

[12] J. Eigeldinger and H. Vogt, "The Bubble Coverage of Gas-Evolving Electrodes in a Flowing Electrolyte," Electrochim. Acta, vol. 45, pp. 4449–4456, 2000.

[13] H. Vogt, "The Supersaturation of Gas in Electrolyte," Electrochim. Acta, vol. 25, pp. 527–531, 1980.

[14] D. Fernandez et al., "Bubble Formation at a Gas-Evolving Microelectrode," Langmuir, vol. 30, pp. 13065–13074, 2014.

[15] A. Angulo et al., "Influence of Bubbles on the Energy Conversion Efficiency of Electrochemical Reactors," Joule, vol. 4, pp. 555–579, 2020.

[16] M. Kibria et al., "Electrochemical CO2 Reduction into Chemical Feedstocks," Nat. Mater., vol. 14, pp. 1099–1118, 2015.

[17] S. Siracusano et al., "Degradation Issues of PEM Electrolysis MEAs," Renew. Energy, vol. 123, pp. 52–57, 2018.

[18] A. J. Bard and L. R. Faulkner, Electrochemical Methods, 2nd ed., Wiley, 2001.

[19] J. Newman and K. E. Thomas-Alyea, Electrochemical Systems, 3rd ed., Wiley, 2004.

[20] P. Trinke et al., "Current Density Singularities in PEM Water Electrolysis," J. Electrochem. Soc., vol. 163, pp. F3164–F3170, 2016.

[21] O. Schmidt et al., "Future Cost and Performance of Water Electrolysis," Int. J. Hydrogen Energy, vol. 42, pp. 13729–13745, 2017.

[22] M. David et al., "Advances in Alkaline Water Electrolyzers," J. Energy Storage, vol. 23, pp. 392–403, 2019.

[23] E. Brauns and T. Turek, "Alkaline Water Electrolysis Powered by Renewable Energy," Processes, vol. 8, p. 248, 2020.

[24] I. Vincent and D. Bessarabov, "Low Cost Hydrogen Production by Anion Exchange Membrane Electrolysis," Renew. Sustain. Energy Rev., vol. 81, pp. 1690–1704, 2018.

[25] F. Schomburg et al., "Lithium-Ion Battery Cell Formation," Energy Environ. Sci., vol. 17, pp. 2686–2733, 2024.

Acknowledgments

The GPC-based electrolysis protocol is protected under PCT/TR2025/051176 and USPTO Application No. 19/298,223. The author is the named inventor. No external funding was received for the preparation of this manuscript.

Declaration of Competing Interest

Ibrahim Karakoc holds intellectual property and commercial rights related to the Generated Pattern Current (GPC) and Dynamic Defined Pattern Charging (DDPC) technology described in this paper through GigaPulse Energy, Izmir, Turkey.

Data Availability

Data will be made available on request.

Declaration on the Use of AI Writing Assistance

The author used AI-assisted writing tools for language editing and manuscript preparation. The scientific content, theoretical analysis, and all intellectual contributions are entirely the work of the author.